Journal of Power Sources 211 (2012) 154–160

Contents lists available at SciVerse ScienceDirect

Journal of Power Sources

journal homepage: www.elsevier.com/locate/jpowsour

# The role of carbon incorporation in $SnO_2$ nanoparticles for Li rechargeable batteries

Seunghoon Nam [a,1], Sungsoo Kim [a,1], Sungun Wi [a], Hongsik Choi [a], Sujin Byun [a], Soon-Mi Choi [a], Sang-Im Yoo [a], Kyu Tae Lee [b,*], Byungwoo Park [a,**]

[a] WCU Hybrid Materials Program, Department of Materials Science and Engineering, Research Institute of Advanced Materials, Seoul National University, Seoul 151-744, Republic of Korea
[b] Interdisciplinary School of Green Energy, Ulsan National Institute of Science and Technology, Ulsan 689-798, Republic of Korea

ARTICLE INFO

*Article history:*
Received 19 January 2012
Received in revised form
14 March 2012
Accepted 17 March 2012
Available online 11 April 2012

*Keywords:*
Li-ion batteries
Tin-dioxide nanoparticle
Carbon coating

ABSTRACT

Since carbothermal reduction of $SnO_2$ occurs above 600 °C, carbon-coating experiments using various polymer precursors have been carried out at relatively low temperatures (~500 °C). It is not likely, however, that the carbon synthesized at ~500 °C much enhances the conductivity of $SnO_2$ anodes, because polymer precursors have undergone insufficient carbonization. This article confirms that the main role of carbon coating is sustaining the domain of each Sn nanoparticle by preventing its aggregation, and thereby improving the cycling performance of $SnO_2$ nanoparticles. The transmission electron microscopy after cycling showing well dispersed Sn nanoparticles and electrochemical impedance spectroscopy revealing larger charge-transfer resistances with increasing carbon contents are in line with these interpretations.



## 1. Introduction

Practical alternatives to the commercial graphite anode in lithium-ion batteries have been investigated extensively to overcome the capacity limitation of graphite (372 mAh $g^{-1}$) [1–4]. Several alternative anode materials with high capacity and stable cycle-life performance appear to be most promising advancement of Li-ion batteries [5–10]. It has been reported that the major drawback of graphite anode could be adequately overcome with the use of $SnO_2$: $SnO_2$ theoretically can store more than twice as much $Li^+$ as graphite (781 mAh $g^{-1}$) [11–15]. $SnO_2$, however, suffers from a large initial irreversible capacity with the formation of $Li_2O$ and from poor capacity retention due to the volume expansion of Sn during electrochemical reactions with $Li^+$ [Eqs. (1) and (2)]. These are the main barriers to the practical utilization of $SnO_2$ [16–18]:

$$SnO_2 + 4Li^+ + 4e^- \rightarrow 2Li_2O + Sn \quad (1)$$

$$Sn + 4.4Li^+ + 4.4e^- \rightleftarrows Li_{4.4}Sn \quad (2)$$

The amorphous $Li_2O$ matrix formed by a conversion reaction [7] is assumed to be electrochemically inert after the first introduction of $Li^+$, but the volume expansion of Sn occurs when it reacts with $Li^+$ in the subsequent alloying–dealloying processes. Courtney et al. [19] observed that small Sn particles aggregated into larger Sn clusters during repeated reversible reaction with lithium. Then, the aggregation of active particles leads to more severe volume expansion of Sn as the absolute changes in dimensions of the active particles become significant [19]. This volume expansion of $Li_xSn$ consequently causes the particles to detach and electrically disconnect. Some efforts have tried to modify the morphology and structure of $SnO_2$ to alleviate its electrochemical disadvantages with various types of $SnO_2$ nanostructures, such as nanowires, nanotubes, and nanopowders [20–23].

Another approach includes the fabrication of $SnO_2$ nanocomposites particularly with carbon-based materials most of which are synthesized from polymer precursors at ~500 °C [13,24–26] (since $SnO_2$ goes through a carbothermal reduction and turns

* Corresponding author. Tel.: +82 52 217 2930; fax: +82 52 217 2909.
** Corresponding author. Tel.: +82 2 880 8319; fax: +82 2 885 9671.
*E-mail addresses:* ktlee@unist.ac.kr (K.T. Lee), byungwoo@snu.ac.kr (B. Park).
[1] Two authors contributed equally to this work.

0378-7753/$ – see front matter © 2012 Elsevier B.V. All rights reserved.
doi:10.1016/j.jpowsour.2012.03.061

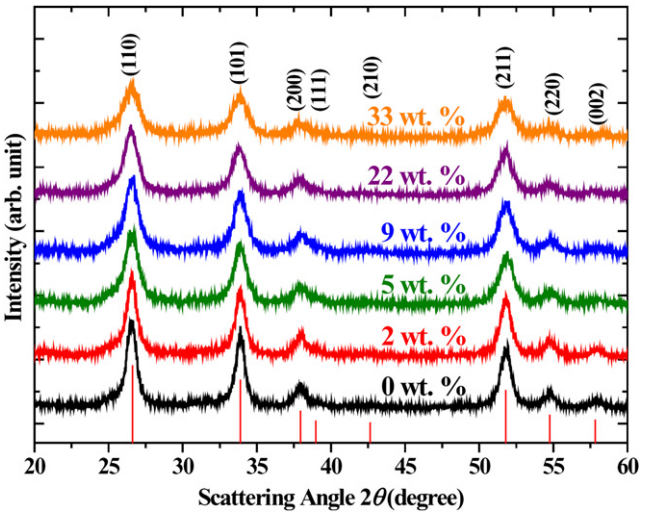


**Fig. 1.** XRD patterns of the $SnO_2$ nanoparticles with different carbon contents. The ideal peak positions and intensities for rutile $SnO_2$ (JCPDS #41-1445) are marked at the bottom.

into Sn metal at or above 600 °C [27]). Most papers have reported that carbon additives not only increase the conductivity of C-coated $SnO_2$ but also serve as a physical buffer layer [28–31]. It is not clear, however, that the enhanced electrical conductivity by these additives indeed plays a dominant role in improving the

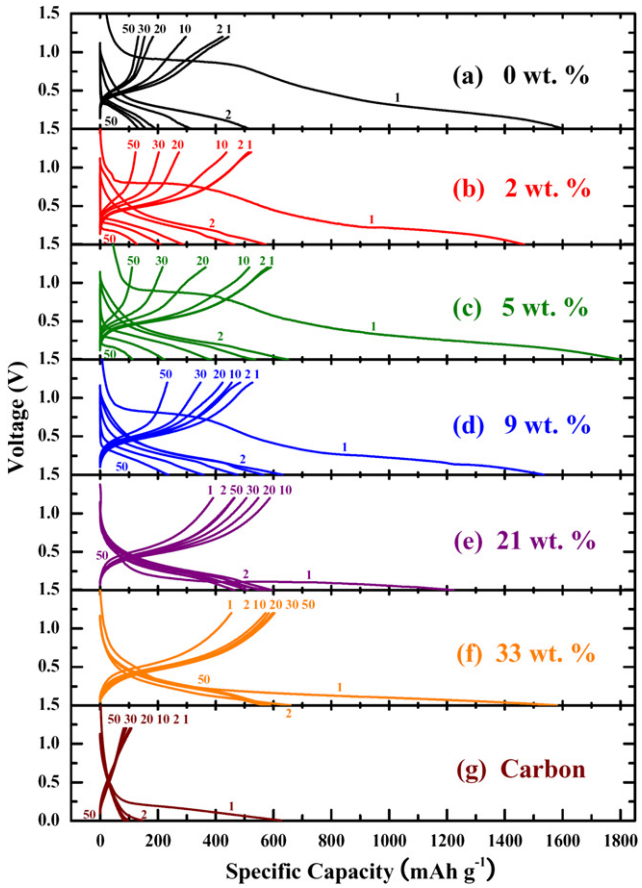


**Fig. 2.** Voltage profiles for the $SnO_2$ nanoparticles with different carbon contents and for disordered carbon only. All of the cells were cycled between 5 mV and 1.2 V at a current density of 500 mA $g^{-1}$ (=0.64 C).

**Table 1**
The compositions and sizes of the $SnO_2$ nanoparticles with different amount of glucose. The compositions were measured by CHNS elemental analysis, and the grain sizes were measured by x-ray diffraction.

| Glucose (g) | $SnO_2$ (wt.%) | C (wt.%) | Grain size (nm) |
|---|---|---|---|
| 0 | 99.98 | 0.02 | 14.2 ± 0.2 |
| 0.5 | 97.55 | 2.45 | 13.8 ± 0.2 |
| 1 | 94.66 | 5.34 | 11.2 ± 0.2 |
| 2 | 91.29 | 8.71 | 10.0 ± 0.1 |
| 4 | 78.39 | 21.61 | 9.5 ± 0.2 |
| 5 | 66.84 | 33.16 | 8.4 ± 0.1 |

electrochemical performance of C-coated $SnO_2$ [32]. Even though various groups [13,24–26] have reported that carbon synthesized at a low temperature (~500 °C) improves $SnO_2$ anodes, demonstrating a primary origin of enhanced cell properties by carbon coating is still lacking. In this respect, this article explains the exact

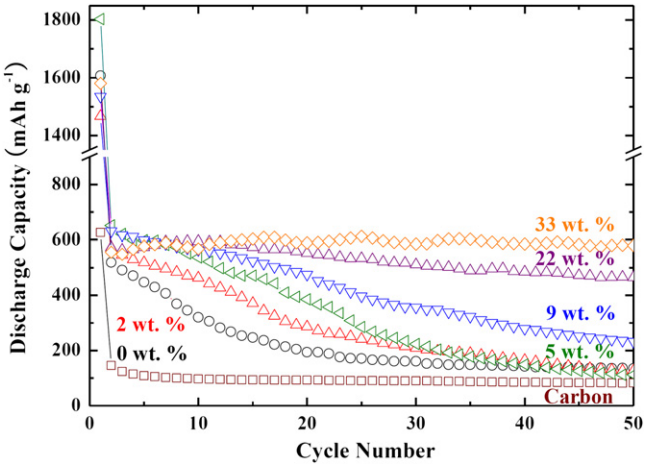


**Fig. 3.** Cycle-life performances of carbon-coated $SnO_2$ nanoparticles with different carbon contents and disordered carbon as an active material, with a current rate of 500 mA $g^{-1}$ (=0.64 C) between 5 mV and 1.2 V.

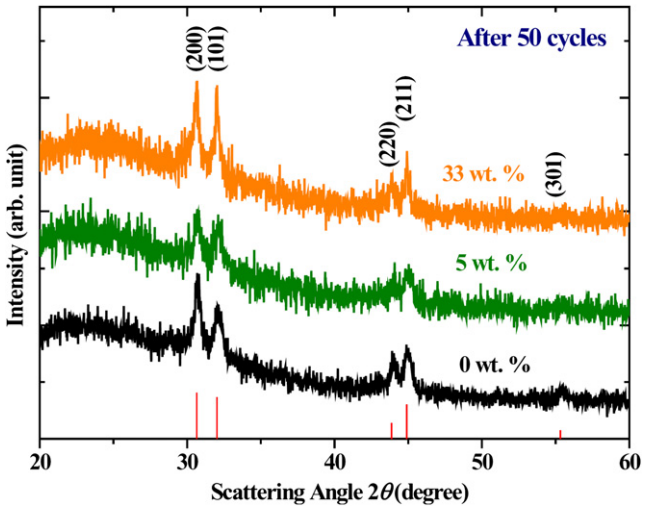


**Fig. 4.** XRD patterns of the $SnO_2$ nanoparticles at 1.2 V as a function of carbon contents, after 50 cycles between 5 mV and 1.2 V. The diffraction patterns are indexed to tetragonal Sn. The ideal peak positions and intensities are marked for tetragonal Sn (JCPDS #04-0673).

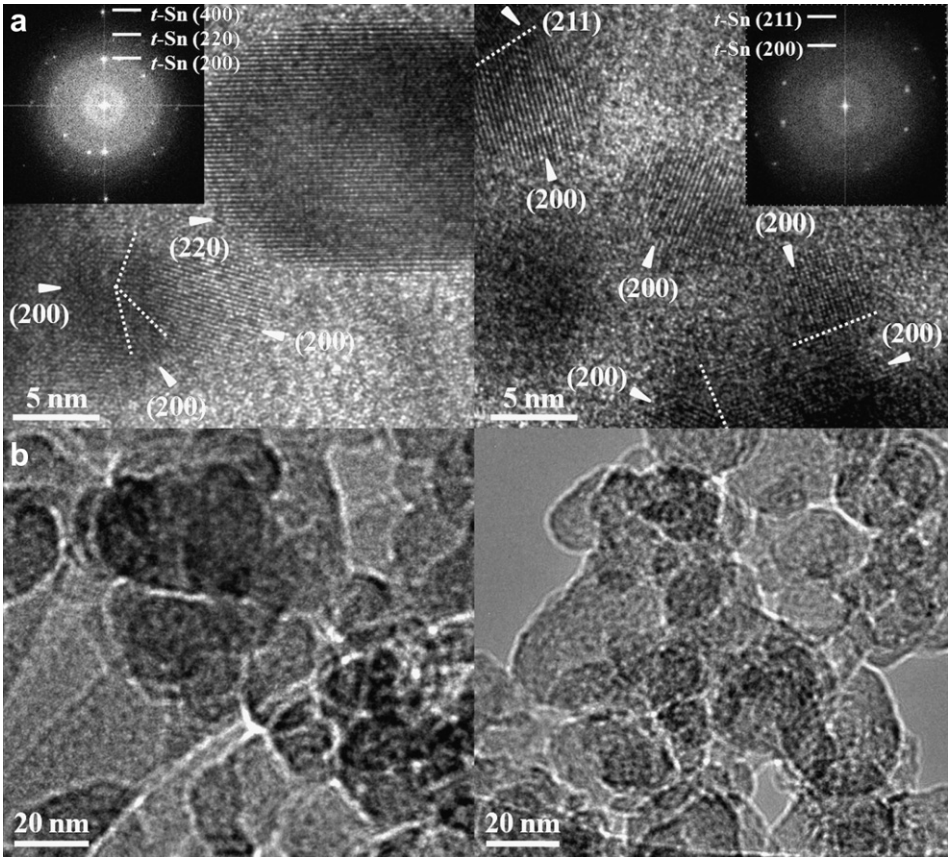


**Fig. 5.** TEM images of uncoated $SnO_2$ nanoparticles at 1.2 V after 50 cycles under different magnifications. The inset images are diffraction patterns showing the tetragonal Sn phase. The orientations of Sn nanoparticles are indicated by solid triangles.

role of carbon in $SnO_2$ nanoparticles during electrochemical reactions by varying the amount of incorporated carbon.

## 2. Experimental procedure

A solvothermal method was adopted to synthesize $SnO_2$ nanoparticles using $SnCl_4$ and ethylene glycol ($C_2H_6O_2$). One milliliter of liquid $SnCl_4$ (Aldrich, 99%) was first dissolved in 40 mL of ethylene glycol (Kanto Chemical, 99.5%), and anhydrous $\alpha$-D-glucose (Aldrich, 96%) ($C_6H_{12}O_6$) (0–5 g) was then added as a carbon source under magnetic stirring [33]. They were heated by a one-step method to effectively coat each nanoparticle and to minimize the amount of organic precursor (glucose) used for subsequent carbonization [34]. The mixtures were kept in a Teflon-sealed autoclave at 180 °C for 12 h. After cooling to room temperature, the resulting precipitates were washed a couple of times in water and ethanol, followed by drying in oven for 10 h. The dried powders were heat-treated under Ar atmosphere at 500 °C for 4 h to obtain C-coated and pure (uncoated, 0 g of glucose) $SnO_2$ nanoparticles. Pure carbon was synthesized with only glucose [35] to estimate the capacity of carbon used in this experiment ($\sim$100 mAh $g^{-1}$). The structure and phase of the $SnO_2$ nanoparticles were identified by x-ray diffraction (XRD: M18XHF-SRA, MAC Science). The relative compositions of carbon were measured using CHNS analyzer (Flash EA 1112, Thermo Electron Corp.). Transmission electron microscopy (TEM) and conventional energy dispersive x-ray (EDX) spectroscopy were performed using a JEM-3000F-JEOL operating at 200 keV accelerating voltage. To prepare samples for TEM analyses, the 50 times-cycled $SnO_2$ nanoparticles were disassembled in a glove box, washed in diethylene carbonate, dried in vacuum, and then washed in ethanol. The resulting solutions were dropped on an amorphous-carbon-coated copper grid and dried in an oven before the analysis.

Cycling tests were performed using coin-type half cells (2016 type) with a Li counter electrode. The Li counter electrode was punched into 1 mm-thick disc with an area of 1.77 $mm^2$. The working electrode consisted of an active material, a super P carbon black, and a polyvinylidene fluoride binder at a weight ratio of 8:1:1. The electrolyte contained 1 M $LiPF_6$ in ethylene carbonate/diethylene carbonate (1/1 vol.%) (Cheil Industries Inc.). The cells were cycled between 5 mV and 1.2 V after the first discharge from the initial open-circuit voltage. The cycling tests were performed at constant current density of 500 mA $g^{-1}$ (=0.64 C rate based on the theoretical capacity of SnO2). The specific capacity was calculated based on the amount of only $SnO_2$, and the capacity of carbon was subtracted in this article. Electrochemical impedance spectra were measured using a potentiostat (CHI 608C: CH Instrumental Inc.) after 5 cycles at 0.64 C. The applied voltage was 0.53 V with AC amplitude of 5 mV in the frequency range from 10 mHz to $10^5$ Hz.

## 3. Results and discussion

The XRD patterns of carbon-coated $SnO_2$ nanoparticles with different carbon contents are exhibited in Fig. 1. All of the diffraction peaks are indexed to $SnO_2$ with the space group *P*42/*mnm* (136) (JCPDS #41-1445), and no secondary phases are detected. The observed broad peaks are indicative of $SnO_2$ nanocrystals. The average grain sizes were estimated by Scherrer equation [36–38] with the peak widths (full width at half

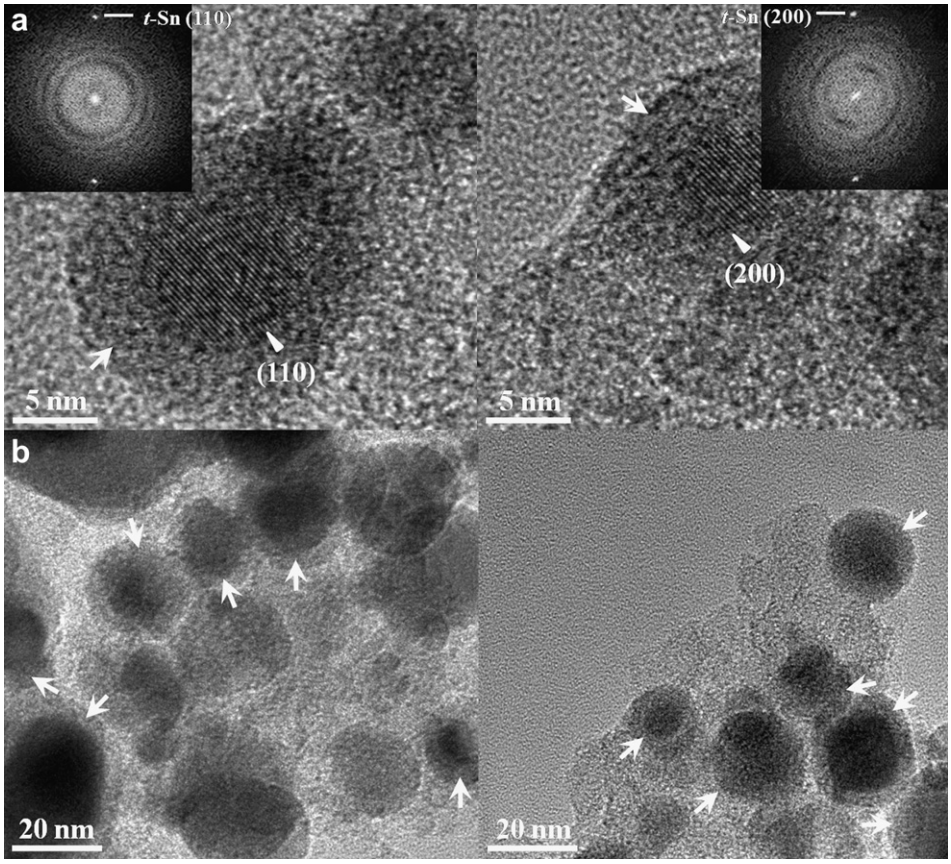


**Fig. 6.** TEM images 33 wt.% C-coated $SnO_2$ nanoparticles at 1.2 V after 50 cycles under different magnifications. The inset images are diffraction patterns showing the tetragonal Sn phase. The orientations of Sn nanoparticles are indicated by solid triangles. The dark-gray region highlighted by arrows consists of probable $Li_2O$ and carbon layer.

maximum) (fitted using a double peak Lorentzian function, considering the effect of $K\alpha_1$ and $K\alpha_2$) corresponding to the (110), (101), and (211) main peaks, and are tabulated in Table 1 for C-coated $SnO_2$ nanoparticles synthesized from different amounts of glucose. It is very likely that linked glucose chains prevent the growth of $SnO_2$, and therefore the grain size of $SnO_2$ becomes smaller with increasing amounts of glucose.

The cycle-life performances of C-coated $SnO_2$ nanoparticles with different carbon contents are presented in Fig. 2. A difference between the uncoated and C-coated samples is observed at the ~0.8 V plateau indicating the formation of the $Li_2O$ phase. This plateau completely vanishes from the ~22 wt.% C-coated $SnO_2$ [39]. It is noted that the carbon used in this article is a disordered carbon with insufficient carbonization [33]. The carbon contents were identified with an elemental analyzer, and are tabulated in Table 1.

The ~33 wt.% C-coated $SnO_2$ nanoparticles maintain the capacity of ~600 mAh $g^{-1}$ until the 50th cycle. The uncoated $SnO_2$ nanoparticles, on the other hand, suffer from a significant loss of capacity only after 20 cycles, giving a discharge capacity of ~150 mAh $g^{-1}$ at the 50th cycle. The $SnO_2$ nanoparticles with intermediate amounts of carbon (~2, ~5, and ~9 wt.%) show slight decreases in their initial capacities followed by high rates of decay leading to comparable capacities to that of the uncoated $SnO_2$ at the 50th cycle. The ~22 wt.% C-coated $SnO_2$ nanoparticles show more stable cycle-life performances, but still exhibit a loss of capacity after 50 cycles. The gradual increases in capacity during the first 10 cycles (Fig. 3(e) and (f)) indicate that it takes some time for the electrolyte to penetrate into $SnO_2$ particles with thick carbon layers (~22 and ~33 wt.% carbon) [40]. Evidently, a certain amount of carbon starts to enhance the cycle-life performance of $SnO_2$ nanoparticles.

It is well known that several disadvantages of a $SnO_2$ anode are mainly due to the large mismatch of volume between Sn and $Li_xSn$. The accommodation of such a volume expansion seems important to secure a large and stable reversible capacity. Therefore, the effective coating of carbon is beneficial for cycling stability of $SnO_2$ nanoparticles. The cycle-life performances of C-coated $SnO_2$ with different amounts of carbon (from ~0 to ~33 wt.%) for 50 cycles are displayed in Fig. 3. The carbon contributes ~100 mAh $g^{-1}$ to the capacity after the initial stages [41].

The cycled $SnO_2$ nanoparticles were examined with both XRD and TEM to confirm the rationale behind the different cycling performances. After the cells were disassembled after 50 cycles, the XRD patterns of C-coated $SnO_2$ nanoparticles were collected, and are shown in Fig. 4. All reflections for the samples are in accordance with a tetragonal Sn (JCPDS #04-0673). The average grain sizes of the samples with ~0 and ~33 wt.% carbon are almost the same, independent of the carbon contents.

The results of XRD are consistent with those of TEM analysis. The images in Fig. 5(a) were obtained from the uncoated $SnO_2$ nanoparticles at 1.2 V after 50 cycles, and the tetragonal Sn (*t*-Sn) nanoparticles were confirmed by electron diffraction. It can be seen that Sn nanoparticles aggregate into larger clusters. As highlighted with dashed lines, several grains are in close proximity to each other, and are likely to clump together into clusters or particles [19,42]. Aggregated particles cause severe volume expansion, and as a result, the active particles crack to release the mechanical

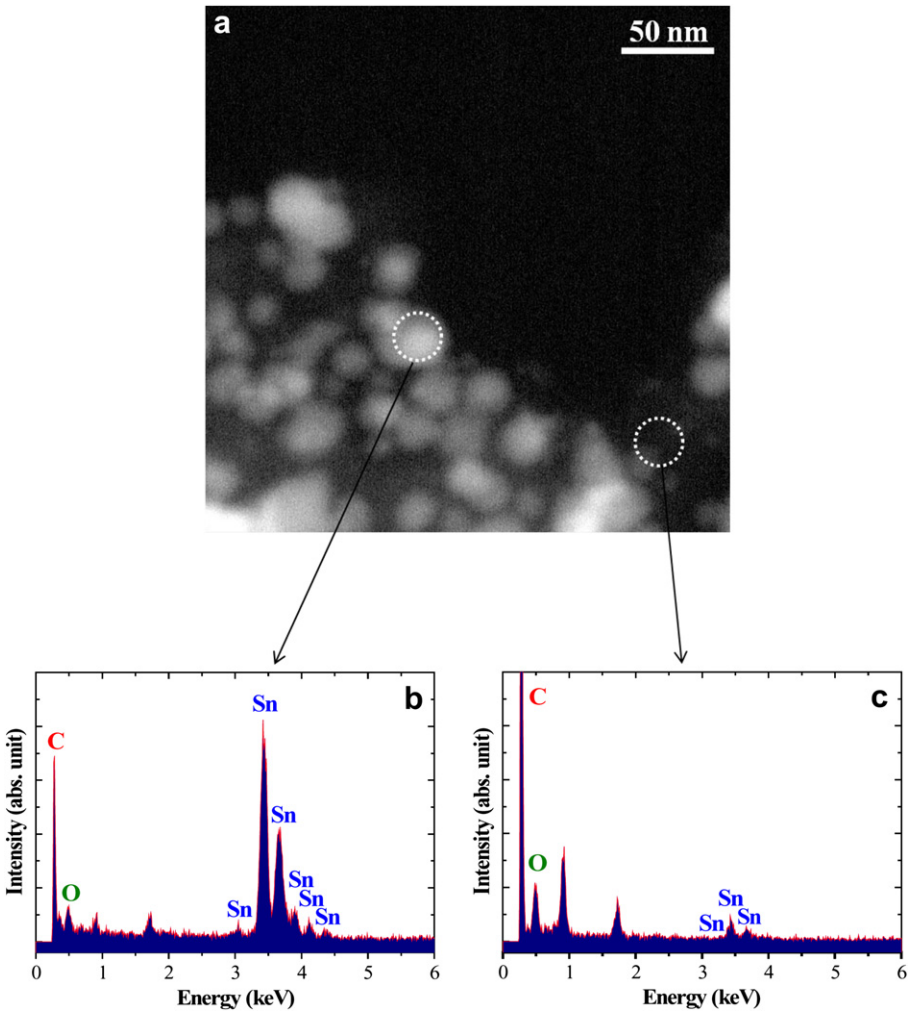


**Fig. 7.** (a) A TEM image of 33 wt.% C-coated $SnO_2$ at 1.2 V after 50 cycles, and the corresponding EDX analyses of (b) bulk regions (Sn rich), and (c) the boundary (carbon and oxygen rich).

stresses during their reactions with $Li^+$ [43,44]. Then, the pulverized particles are exposed to the electrolyte to form a new solid electrolyte interphase (SEI), and/or become electrically disconnected, which are the main causes of capacity fade in $SnO_2$ anodes [45]. The images in Fig. 5(b) also show rather aggregated states of particles.

On the other hand, the images of ~33 wt.% C-coated $SnO_2$ nanoparticles exhibit each single grain coated with carbon, as shown in Fig. 6. The observed core–shell structure is established by a coating layer which consists of probable $Li_2O$ and carbon. Interestingly, the image shows solid core/shell morphology even though the volume contraction from $LiSn_x$ to Sn should have resulted in rather a hollow core structure. One possibility for this is that Sn oxidizes in air during the sample preparation for TEM [42]. From Fig. 6, it appears that the gel-like $Li_2O$ within the shell is squeezed out: it is evident that $Li_2O$ itself serves as a buffer during the volume expansion of $LiSn_x$ [46]. Both $Li_2O$ and carbon help to accommodate the volume expansion, with the carbon also preventing Sn from migrating to the neighboring particles. Thus, the Sn nanoparticles with ~33 wt.% carbon coating have difficulty in aggregating. The EDX analysis of the bulk (Fig. 7(b)) shows that core part of the particles is mainly composed of Sn, whereas regions nearest the boundaries (Fig. 7(c)) confirm that some phases containing oxygen, which are likely to be $Li_2O$ and some amounts of possible $SnO_2$, are the main components of the shell. It should be noted that carbon is also expected within the shell, despite the low detection limit of carbon by EDX.

The estimated thickness of carbon in ~33 wt.% C-coated Sn nanoparticles is approximately 2 nm with the densities of disordered carbon (hard carbon ≅ 1.5 g $cm^{-3}$) [47] and tin oxide (6.95 g $cm^{-3}$), assuming a complete carbon encapsulation of spherical $SnO_2$ nanoparticles (~8.4 nm in diameter). With an essential amount of carbon layer (approximately ~2 nm), superior electrochemical stability is obtained by reversible volume change with little aggregation of Sn nanoparticles during cycling.

Particularly important is the electrochemical impedance spectra of C-coated $SnO_2$ nanoparticles with different carbon contents. The Nyquist plot in Fig. 8(a) reveals the impedances associated with the charge-transfer resistances of the C-coated $SnO_2$. The charge-transfer resistance ($R_{ct}$), which is believed to be one of the important factors in electrochemical reactions, is reflected in the diameter of the semicircle along the $Z'$ axis [48]. The inset in Fig. 8(b) shows an approximated equivalent circuit of C-coated $SnO_2$: the solution resistance, charge-transfer resistance, constant-phase element, and Warburg impedance are denoted by $R_s$, $R_{ct}$, CPE, and $Z_w$, respectively. The charge-transfer resistances of C-coated $SnO_2$ were obtained by fitting the spectra based on the equivalent circuit. The Nyquist plot demonstrates that more carbon contents result in

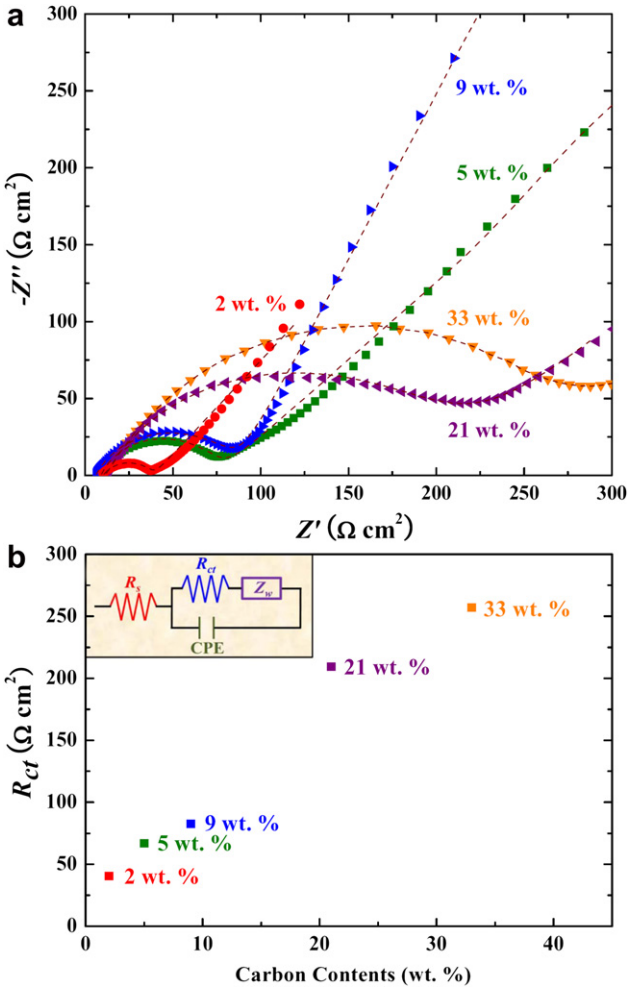


**Fig. 8.** (a) Electrochemical impedance spectroscopy of C-coated $SnO_2$ after 5 cycles with an applied voltage of 0.53 V. The fitting lines were obtained using the equivalent circuit below. (b) The charge-transfer resistances of C-coated $SnO_2$ with increasing carbon contents.

higher charge-transfer resistance. This, however, seems contradictory since the cycling stability clearly improves with the amount of carbon. One plausible explanation could be that the carbon layer synthesized from a polymer precursor, with relatively low-temperature (500 °C) calcination, does not contribute much to the conductivity of the active particles [32,39]. It has been reported that carbon synthesized at a temperature lower than 700 °C still has some amounts of hydrogen and oxygen present, leaving $sp^3$ local bonding of the host carbon atoms [49,50].

The evolution of nanostructures during electrochemical lithiation/delithiation processes is illustrated. As shown in Fig. 9, it can be concluded that the cycling properties are enhanced by little aggregation of active materials with the aid of the coated carbon. The key factor controlling the reversibility is the sustaining of the domain of each nanoparticle, by limiting the possible aggregations among them [18]. In other words, the degree of Sn-nanoparticle aggregation is more likely to determine the capacity retention. More detailed *in situ* experiments are needed to clarify the exact mechanisms of the lithiation process and of the insulating characteristics of the carbon layer enhancing the cycle-life performance of $SnO_2$ anodes [51].

## 4. Conclusions

Of the C-coated $SnO_2$ nanoparticles synthesized with different amounts of glucose, the ~33 wt.% C-coated $SnO_2$ nanoparticles exhibit a superior cycling stability compared to the others, and they maintain a capacity of ~600 mAh $g^{-1}$ until the 50th cycle. Since the C-coated $SnO_2$ nanoparticles are synthesized under the solvothermal condition and further heated to 500 °C, the effect of electrical conductivity of carbon on the electrochemical performance can be moderately excluded. The TEM images after cycling confirm that the nanoparticles are well dispersed with little aggregation. The electrochemical impedances, together with the images from TEM verify that the most significant role of carbon in C-coated $SnO_2$ is to sustain the domain of each Sn nanoparticle so that more facile accommodation of volume expansion of $Li_xSn$ can be achieved during the electrochemical lithiation/delithiation processes.

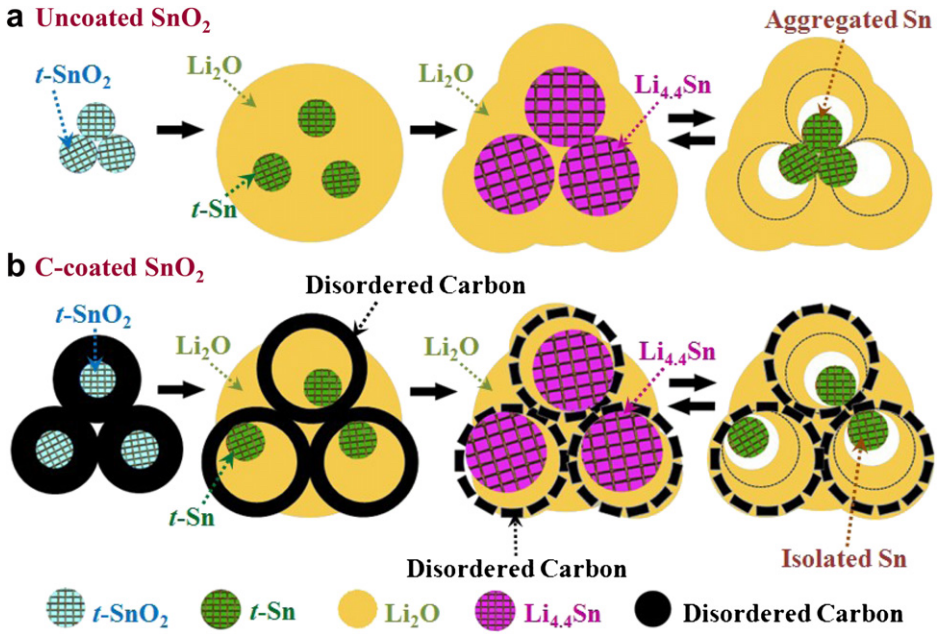


**Fig. 9.** Schematic illustrations showing the evolution of nanostructures during the electrochemical lithiation/delithiation processes.

## Acknowledgments

This research was supported by the National Research Foundation of Korea Grant funded through the Korean Government (MEST: NRF, 2010-0029065) and the World Class University (WCU, R31-2008-000-10075-0).

## References

[1] E. Peled, C. Menachem, D. Bar-Tow, A. Melman, J. Electrochem. Soc. 143 (1996) L4–L7.
[2] J.-G. Lee, D. Son, C. Kim, B. Park, J. Power Sources 172 (2007) 908–912.
[3] X. Chen, K. Gerasopoulos, J. Guo, A. Brown, C. Wang, R. Ghodssi, J.N. Culver, ACS Nano 4 (2010) 5366–5372.
[4] D. Ahn, C. Kim, J.-G. Lee, B. Park, J. Solid State Chem. 181 (2008) 2139–2142.
[5] K. Amine, I. Belharouak, Z. Chen, T. Tran, H. Yumoto, N. Ota, S.-T. Myung, Y.-K. Sun, Adv. Mater. 22 (2010) 3052–3057.
[6] H.-W. Ha, S.-J. Hwang, Electrochim. Acta 55 (2010) 2841–2847.
[7] P. Poizot, S. Laruelle, S. Grugeon, L. Dupont, J.-M. Tarascon, Nature 407 (2000) 496–499.
[8] K.T. Lee, Y.S. Jung, S.M. Oh, J. Am. Chem. Soc. 125 (2003) 5652–5653.
[9] Y. Yao, J. Chang, L. Xue, T. Huang, A. Yu, J. Power Sources 196 (2011) 10240–10243.
[10] Z. Wei, Z. Liu, R. Jiang, C. Bian, T. Huang, A. Yu, J. Solid State Electrochem. 14 (2010) 1045–1050.
[11] Y. Idota, T. Kubota, A. Matsufuji, Y. Maekawa, T. Miyasaka, Science 276 (1997) 1395–1397.
[12] L.-S. Zhang, L.-Y. Jiang, H.-J. Yan, W.D. Wang, W. Wang, W.-G. Song, Y.-G. Guo, L.-J. Wan, J. Mater. Chem. 20 (2010) 5462–5467.
[13] J. Liu, W. Li, A. Manthiram, Chem. Commun. 46 (2010) 1437–1439.
[14] J. Ye, H. Zhang, R. Yang, X. Li, L. Qi, Small 6 (2010) 296–306.
[15] C. Zhong, J. Wang, Z. Chen, H. Liu, J. Phys. Chem. C 115 (2011) 25115–25120.
[16] J.O. Besenhard, J. Yang, M. Winter, J. Power Sources 68 (1997) 87–90.
[17] L.Y. Beaulieu, K.W. Eberman, R.L. Turner, L.J. Krause, J.R. Dahn, Electrochem. Solid-State Lett. 4 (2001) A137–A140.
[18] I.A. Courtney, J.R. Dahn, J. Electrochem. Soc. 144 (1997) 2943–2948.
[19] I.A. Courtney, W.R. McKinnon, J.R. Dahn, J. Electrochem. Soc. 146 (1999) 59–68.
[20] N. Li, C.R. Martin, J. Electrochem. Soc. 148 (2001) A164–A170.
[21] H.-J. Ahn, H.-C. Choi, K.-W. Park, S.-B. Kim, Y.-E. Sung, J. Phys. Chem. B 108 (2004) 9815–9820.
[22] M.-S. Park, G.-X. Wang, Y.-M. Kang, D. Wexler, S.-X. Dou, H.-K. Liu, Angew. Chem. 119 (2007) 764–767.
[23] Y. Wang, H.C. Zeng, J.Y. Lee, Adv. Mater. 18 (2006) 645–649.
[24] X.W. Lou, D. Deng, J.Y. Lee, L.A. Archer, Chem. Mater. 20 (2008) 6562–6566.
[25] J.S. Chen, Y.L. Cheah, Y.T. Chen, N. Jayaprakash, S. Madhavi, Y.H. Yang, X.W. Lou, J. Phys. Chem. C 113 (2009) 20504–20508.
[26] H. Qiao, Z. Zheng, L. Zhang, L. Xiao, J. Mater. Sci. 43 (2008) 2778–2784.
[27] X. Sun, J. Liu, Y. Li, Chem. Mater. 18 (2006) 3486–3494.
[28] S.H. Ng, J.Z. Wang, D. Wexler, K. Konstantinov, Z.P. Guo, H.K. Liu, Angew. Chem. Int. Ed. 45 (2006) 6896–6899.
[29] G. Derrien, J. Hassoun, S. Panero, B. Scrosati, Adv. Mater. 19 (2007) 2336–2340.
[30] M.S. Park, S.A. Needham, G.X. Wang, Y.M. Kang, J.S. Park, S.X. Dou, H.K. Liu, Chem. Mater. 19 (2007) 2406–2410.
[31] B. Zhang, Q.B. Zheng, Z.D. Huang, S.W. Oh, J.K. Kim, Carbon 49 (2011) 4525–4534.
[32] L. Wang, G.C. Liang, X.Q. Ou, X.K. Zhi, J.P. Zhang, J.Y. Cui, J. Power Sources 189 (2009) 423–428.
[33] T. Moon, C. Kim, S.-T. Hwang, B. Park, Electrochem. Solid-State Lett. 9 (2006) A408–A411.
[34] Z. Chen, J.R. Dahn, J. Electrochem. Soc. 149 (2002) A1184–A1189.
[35] X. Sun, Y. Li, Angew. Chem. Int. Ed. 43 (2004) 597–601.
[36] T. Kim, J. Oh, B. Park, K.S. Hong, Appl. Phys. Lett. 76 (2000) 3043–3045.
[37] D. Son, D.-R. Jung, J. Kim, T. Moon, C. Kim, B. Park, Appl. Phys. Lett. 90 (2007) 101910–101913.
[38] D.-R. Jung, D. Son, J. Kim, C. Kim, B. Park, Appl. Phys. Lett. 93 (2008) 163118–163121.
[39] M. Noh, Y. Hwon, H. Lee, J. Cho, Y. Kim, M.G. Kim, Chem. Mater. 17 (2005) 1926–1929.
[40] X.-L. Wu, L.-Y. Jiang, F.-F. Cao, Y.-G. Guo, L.-J. Wan, Adv. Mater. 21 (2009) 2710–2714.
[41] E. Kim, Y. Kim, M.G. Kim, J. Cho, Electrochem. Solid-State Lett. 9 (2006) A156–A159.
[42] C. Kim, M. Noh, M. Choi, J. Cho, B. Park, Chem. Mater. 17 (2005) 3297–3301.
[43] H. Mukaibo, T. Momma, Y. Shacham-Diamand, T. Osaka, M. Kodaira, Electrochem. Solid-State Lett. 10 (2007) A70–A73.
[44] M. Winter, J.O. Besenhard, Electrochim. Acta 45 (1999) 31–50.
[45] M. Inaba, T. Uno, A. Tasaka, J. Power Sources 146 (2005) 473–477.
[46] A. Sivashanmugam, T.P. Kumar, N.G. Renganathan, S. Gopukumar, M. Wohlfahrt-Mehrens, J. Garche, J. Power Sources 144 (2005) 197–203.
[47] H. Azuma, H. Imoto, S. Yamada, K. Sekai, J. Power Sources 81–82 (1999) 1–7.
[48] B. Lee, C. Kim, Y. Park, T.-G. Kim, B. Park, Electrochem. Solid-State Lett. 9 (2006) E27–E30.
[49] V. Palomares, A. Goni, I.G. De Muro, I. De Meatza, M. Bengoechea, I. Cantero, T. Rojo, J. Electrochem. Soc. 156 (2009) A817–A821.
[50] M. Kumar, R.C. Gupta, J. Mater. Sci. 28 (1993) 440–444.
[51] B. Kim, C. Kim, D. Ahn, T. Moon, J. Ahn, Y. Park, B. Park, Electrochem. Solid-State Lett. 10 (2007) A32–A35.